CPT: Pharmacometrics & Systems Pharmacology

ARTICLE OPEN ACCESS

A Unified Whole Lung PBK Model for Inhalational Uptake of Gases and Aerosols in Men

Norman Nowak | Sylvia E. Escher | Katharina Schwarz

Fraunhofer ITEM, Hannover, Germany

Correspondence: Katharina Schwarz (katharina.schwarz@item.fraunhofer.de)

Received: 21 January 2025 | **Revised:** 29 August 2025 | **Accepted:** 8 September 2025

Funding: This research was supported by the Cefic LRI-B21 project, funded by the CEFIC Long-range Research Initiative, and the RISK-HUNT3R project, which received funding from the European Commission's Horizon 2020 research and innovation program.

Keywords: ADME | in silico | in vitro to in vivo | PBK modeling | respiratory pharmacokinetics

ABSTRACT

Assessing the risk or benefit of an inhaled substance is challenging due to the variety of forms it can take (gas, vapor, particle, or droplet) and the complex biological processes involved in its uptake and retention. Physiologically based kinetic (PBK) models offer an alternative to in vivo experiments. However, PBK models for inhalational uptake are to date either designed for gases/vapors or airborne particulates, often with only low regional compartmentalization. The here-presented, newly developed model combines both applications. Its mechanisms are an amalgamation of PBK and non-PBK models integrated into a multicompartmental description of the human lung to include the relevant uptake and clearance processes in the different lung regions, of which macrophage-mediated dissolution is novel to PBK modeling. The model was designed to use a minimal number of substance-specific input parameters, which can be derived from in vitro assays or in silico methods. Model predictions for hypothetical substances with varying physicochemical properties were performed, along with rudimentary sensitivity analyses to identify the most important parameters for gases/vapors and particles. This novel PBK model combines all these aspects and provides in silico predictions of systemic and local lung concentrations, reducing uncertainty in risk assessments and supporting drug development. It serves as a valuable tool to translate nominal ambient air doses into effective localized doses within the lung.

1 | Introduction

The lung is the major portal of entry for gases, vapors, and airborne particles. It is consequently an organ with a complex anatomy and physiology. The nominal dose of an inhaled substance (i.e., ambient air concentration) is, for that reason, an insufficient metric to assess adverse or beneficial responses. Understanding the actual or effective dose within the lung is therefore critical for toxicologists and pharmacologists. However, direct in vivo measurements are often inaccessible. Instead, assumptions, such as full absorption of chemicals in the respiratory tract, are used for chemical hazard assessments when substance-specific data are unavailable [1]. Physiologically based kinetic (PBK) modeling can refine these default assumptions, offering a more accurate prediction of substance bioavailability.

PBK models are mathematical frameworks that simulate the distribution of substances within an organism. These models divide the body into interconnected compartments representing different tissues and incorporate ADME processes (absorption, distribution, metabolism, excretion). Required input parameters can be categorized as physiological (e.g., tissue volumes, blood flows), chemical-specific (physico- and biochemical properties), and exposure-related. QIVIVE (quantitative in vitro to in vivo) PBK models are "bottom-up" models which use ADME data derived from in vitro and in silico approaches,

Study Highlights

- What is the current knowledge on the topic?
  - Existing PBK models for inhalational uptake are typically specific to gases, vapors, or particles, with limited regional lung compartmentalization. Most models focus on predicting systemic concentrations, often neglecting localized lung dynamics and mechanisms like macrophage-mediated particle dissolution.
- What question did this study address?
  - How can a unified PBK model predict inhalational uptake, retention, and systemic distribution of gases, vapors, and particles, considering lung compartmentalization and diverse physicochemical properties?
- What does this study add to our knowledge?
  - This study presents a comprehensive PBK model incorporating multiple lung compartments to simulate uptake, retention, and clearance mechanisms including longitudinal diffusion and novel macrophage-mediated particle dissolution. It integrates parameters obtainable through NAMs, enabling systemic and localized predictions across various scenarios.
- How might this change drug discovery, development, and/or therapeutics?
  - The model enhances inhalation risk assessments, facilitates targeted drug delivery system designs, and supports translational research by providing detailed in silico predictions of localized lung effects and systemic exposure.

allowing for predictions based on new approach methodologies (NAMs) [2, 3]. NAMs are non-animal scientific techniques and tools, such as in vitro assays and computational models, developed to assess chemical safety without relying on traditional animal testing according to the 3R principle [3]. QIVIVE and NAMs are integral to next-generation risk assessment (NGRA) [3] of using human-relevant, exposure-led, and hypothesis-driven testing. Typical in vitro assays for inhalation measure the apparent permeability of the lung barrier. For example, in vitro assays for inhalation use alveolar or tracheobronchial cell lines to measure lung permeability in submersed or air-liquid interface setups [4]. These data are extrapolated to the in vivo context through QIVIVE. PBK models can also be used to extrapolate between different species by changing the underlying physiological data [5] or to a target substance by filling data gaps with a validated, structurally or functionally analogous substance using read-across [6].

The first model for inhalational uptake described gas uptake in the human lung and blood [7]. Subsequent efforts incorporated mechanisms such as cyclic breathing [8], mucus absorption [9], and permeation and metabolism in the air-blood barrier [10]. Still not addressed is longitudinal diffusion along airways, which replaces convective flow as the dominant mechanism in the deep lung.

While chemical-specific models are highly accurate for individual substances, they lack generalizability for other chemicals or drug formulations. This limitation has spurred the development of generalized PBK models. Generalized models for vapor uptake have evolved, with early semi-empirical models demonstrating reasonable predictive capabilities [11]. However, their applicability remains limited by the chemical space of the parametrization data. A recent advancement is the httk (high-throughput toxicokinetics) model published by the US EPA, which enables broad chemical screening using simplified parameters [12].

Describing the lung with more than a single, homogeneous compartment for the alveolar region was already introduced much earlier by Johanson [9]. Johanson considered the inclusion of multiple airway compartments necessary to adequately model the uptake of hydrophilic substances, which are readily absorbed in the conducting airways. While not a PBK model, as it is not entirely physiologically based, the semi-empirical and revised human respiratory tract model (HRTM) of the ICRP (International Commission on Radiological Protection) [13, 14] compartmentalizes the respiratory tract to predict particular uptake and clearance.

More detailed models, particularly those designed for aerosolized pharmaceuticals, incorporate sub-compartments of the lung to account for its heterogeneity, describing either different lung lobes [15] or lung generations for aerosol uptake [16, 17]. These subdivisions improve estimates of local deposition and total uptake while addressing the lung's structural and functional complexity.

Current PBK models prioritize predicting blood and urine concentrations, often omitting mechanisms relevant to very short or long timeframes. For example, alveolar macrophages play a critical role in particle clearance over years and may influence particle dissolution due to their acidic environment [18]. Similarly, irritant gases can cause damage within minutes of inhalation [19].

A unified PBK model for both gases and aerosols is necessary to address these gaps. The proposed model introduces a multicompartmental framework for predicting inhalational uptake of gases, vapors, and aerosols in both liquid and solid forms. Key improvements include longitudinal diffusion, which facilitates mixing in the deep lung, and the role of alveolar macrophages in particle dissolution. Parameter studies highlight the model's sensitivity to physicochemical properties, demonstrating its applicability across various exposure scenarios. This generalized approach represents a significant step forward in understanding inhalation toxico- and pharmacokinetics and supports more comprehensive risk assessments.

2 | Methods

Gases and vapors behave identically regarding inhalational uptake and will be used interchangeably in this publication.

2.1 | Model Structure

2.1.1 | Physiology

The model describes the lung as a multicompartmental organ divided into 25 lung generations (G1 to G25) according to Yeh and Schum's symmetrical lung geometry model [20], categorized

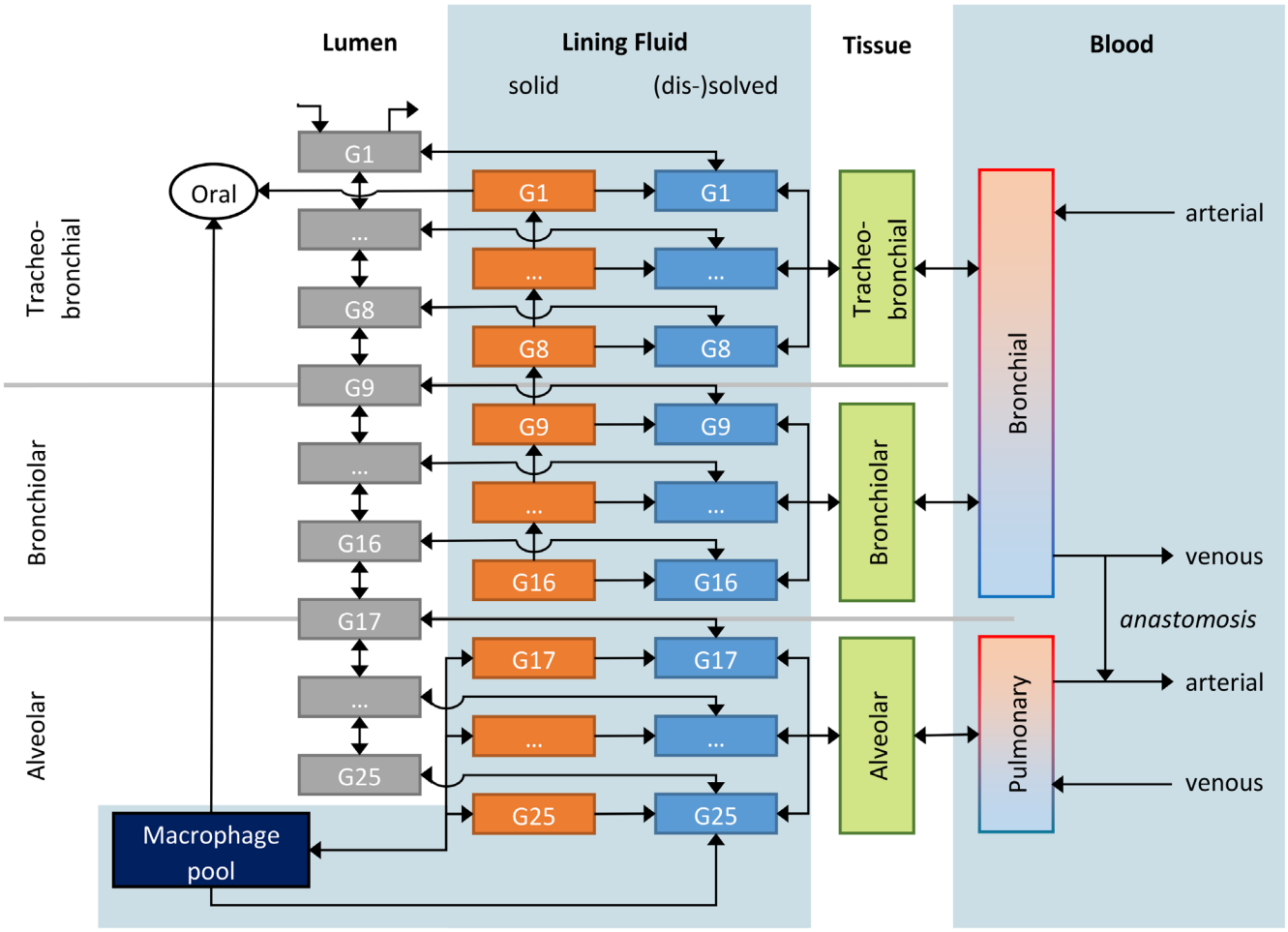

FIGURE 1 | Model structure comprising 25 sections of particle, epithelial lining fluid (ELF) and air lumen compartments to describe the human lung. Compartments are interconnected by mucociliary clearance, particle dissolution in ELF and macrophages, macrophage uptake and clearance, and consecutive diffusion through epithelial and endothelial cell layers.

into three broader regions (Figure 1). Generations 1–16 represent the conducting airways starting at the trachea (G1) and continuing to the bronchi and bronchioles, ending at the terminal bronchioles (G16). The remaining generations 17–25 account for the respiratory airways. G24 represents alveolar sacs, and G25 represents all alveoli lumped together.

Airways are considered hollow cylinders with a concentric, three-layered structure: airway lumen for gas uptake, epithelial lining fluid (ELF) with compartments for deposited particles and (dis)solved substances, and lung tissue. Tissue compartments are shared between generations of the same region and represent epithelium, subepithelial tissue, interstitial space, and endothelium (not explicitly modeled). Tissues are perfused by the bronchial and pulmonary circulation [21]. The pulmonary circulation transports deoxygenated blood from the venous blood pool to the respiratory airways and oxygenated blood back into the arterial blood pool. The bronchial circulation is part of the systemic circulation and supplies oxygenated blood from arterial blood to the conducting airways, from where deoxygenated blood drains into the venous blood. However, due to intrapulmonary shunting/anastomosis, approximately 67% of the blood from the bronchial veins is drained into arterial blood [22].

The lung is connected to the systemic part of the PBK model, which consists of 11 permeability-limited tissue compartments: heart, brain, muscle, skin, kidneys, gastrointestinal tract (GIT), spleen, liver, bone, fat, and separate arterial and venous blood compartments (Figure S1). The structure and equations employed in the systemic part, as well as the underlying physiological data, are described in Appendix S1 in further detail.

2.1.2 | Gas Modeling

Lung compartments are interconnected by a variety of interactions. An inhaled gas flows along airway lumina due to respiration (convection) and diffusion. Diffusion also governs the absorption into ELF and subsequent passage across the epithelium and endothelium into tissue and capillary blood, respectively. Cross-tissue diffusion between lung generations is not explicitly modeled but is indirectly accounted for within a lung region by the three lumped and well-stirred (immediate mixing) tissue compartments.

The thickness of ELF, consisting of a thick mucus layer in the upper airways and a thin, surfactant-containing fluid film in the deep airways, scales down with increasing airway generation.

2.1.3 | Aerosol Modeling

Particles and droplets deposit on the lung's surface. While droplets, once deposited, are treated identically to an absorbed gas, particles are submerged in ELF in which they can dissolve. Slowly dissolving or bioinert particles are removed by mucociliary clearance in the upper airways or phagocytized by alveolar macrophages in the pulmonary region. Phagocytized particles are either dissolved inside macrophages, released back to ELF due to apoptosis, or cleared by slow migration of loaded macrophages to the upper respiratory tract. Particles cleared by the mucociliary escalator or macrophages are subsequently swallowed. Secondary uptake over the gastrointestinal tract is not considered.

2.1.4 | Usage

In total, the here described lung consists of 81 compartments. Despite its complexity, the number of additional parameters required to run the model is quite low and even less when considering only one substance class (gas/vapor, particle, or droplet). However, computations are possible for any combinations of them with different exposure or dosing regimens. Inputs were designed to be obtainable by available NAMs, thus enabling a full QIVIVE or bottom-up model. The substances' specific input parameters can be roughly separated into bio- and physicochemical parameters and application-specific parameters dependent on the exposure scenario. A complete list is shown in Table 1. Note that knowledge of the complete set of parameters is usually not required, for example, gas diffusion coefficients are not necessary for aerosols; dissolution rate constants are only applicable to solid particles.

The model was implemented in R (v4.2.2) and utilizes the R package deSolve (v1.34) [23] to solve the ordinary differential equations numerically. A detailed description of the model's underlying mechanisms and equations is given in Appendix S2.

2.2 | Model Parametrization

Physiological parameters on extrapulmonary tissues are representative for a standard-sized adult man (73 kg) according to reference data [24]. Lung parameters were largely taken from Yeh and Schum [20] based on the findings on a silicon lung cast (male, 60 years, 81 kg). Breathing parameters for a resting person, that is, a typical tidal volume and breathing frequency of 750 mL and 12 breaths/min, were used. Further information on the employed physiological data can be found in Appendix S1. Regarding chemical-specific parameters, instead of modeling a specific substance, hypothetical substances with a range of different physiochemical properties were used. A summary of their values is listed in Table S1.

The Henry's law constant describes the equilibrium concentrations of a substance between its aqueous solution and air. Plausible value ranges for Henry's law constant, water solubility, and diffusion coefficients in air and water were identified from literature (Figure S2). For Henry's law constant (for water as solvent), experimentally measured values at 25°C were retrieved from a compiled database including 2848 entries of inorganic species, hydrocarbons and other organic substances [25]. Experimentally measured and predicted diffusion coefficients in air and water were extracted from a dataset containing 4770 and 2979 entries for organic compounds (1–100 carbon atoms), respectively [26]. The upper limit of these parameters was defined as the third quartile (Q_3) plus the interquartile range ($Q_3 - Q_1$) for the purpose of this study. Lower limits were respectively defined as $Q_1 - (Q_3 - Q_1)$. Diffusion coefficients in air and water show a relatively narrow spread of possible values (within an order of magnitude), with water coefficients being approximately four orders of magnitude smaller than those in air. The water diffusion coefficient has therefore been fixed to $D_{water} = D_{air} \cdot 10^{-4}$.

For the parameter study on gas uptake, the model's sensitivity to the Henry's law constant and the diffusion coefficients in air and water was explored, as these parameters directly relate to the new model description of the lung. The absorption of gases or vapors by inhalation is influenced by multiple factors, including their solubility in the lining fluid, the vapor pressure of the substance dissolved in the fluid (quantified by Henry's law constant, representing the equilibrium between the gaseous and aqueous phases), and their diffusion properties in both air and water (cf. equation S14 + S15). The following value ranges are considered:

- Henry's law constant (H^{cp}): Equilibrium between the gaseous and aqueous phases. It has a lower limit of $7.30 \cdot 10^{-7}$ mol/Pa/m^3, a median value of $1.60 \cdot 10^{-2}$ mol/Pa/m^3, and an upper limit of $5.92 \cdot 10^{2}$ mol/Pa/m^3.
- Diffusion coefficient in air (D_{air}): The values range from $2.40 \cdot 10^{-2}$ cm^2/s (lower limit) to $1.05 \cdot 10^{-1}$ cm^2/s (upper limit), with a median value of $6.29 \cdot 10^{-2}$ cm^2/s.
- Diffusion coefficient in water (D_{water}): The range spans from $2.39 \cdot 10^{-6}$ cm^2/s (lower limit) to $1.15 \cdot 10^{-5}$ cm^2/s (upper limit), with a median value of $7.02 \cdot 10^{-6}$ cm^2/s.

For the particle retention study, particle size and dissolution rate were varied for the same reason. Required deposition fractions were obtained from the Multiple-Path Particle Dosimetry (MPPD) model (v3.04) [27]. Bioinert particles were distributed among lung generations accordingly (Figure S4).

While this data was used to inform the respective parameter studies, assumptions were made for solubility and cell permeability, which can also have an impact on uptake, as briefly described below:

- The solubility limit in water was set to an extremely high number, effectively deactivating its influence on gas uptake.
- To avoid any buildup within the lung due to slow diffusion into the blood system, a very high apparent permeability of $1 \cdot 10^{-5}$ cm/s for the epithelial cell layer was chosen. This way, the influence of the cell barrier on lung concentrations was reduced to a minimum. The permeability of the endothelial cell layer was set arbitrarily to twice the permeability of the epithelium, as it is more permeable than the epithelial layer [28].

TABLE 1 | Chemical-specific and scenario-dependent input parameters for the model.

	Parameter	Symbol	Unit	Type		
				Gas/vapor	Droplet	Particle
Administration	Initial masses[a]	$m_{\text{init},j}$	μg	✓	✓	✓
	External gas concentration	c_{gas}	mg/m^3	✓	✗	✗
	Deposition rates (droplets)[b]	$J_{\text{droplet},i}$	μg/min	✗	✓	✗
	Deposition rates (particles)[b]	$J_{\text{ptcls},i}$	μg/min	✗	✗	✓
Physicochemical	Solubility limit	c_{max}	mg/mL	✓	✗	✓
	Henry's law constant	H^{cp}	mol/Pa/m^3	✓	✗	✗
	Initial particle size	$d_{\text{ptcl\_init}}$	μm	✗	✗	✓
	Particle density	ρ_{ptcl}	g/cm^3	✗	✗	✓
	Gas diffusion coefficient in air	D_{air}	cm^2/s	✓	✗	✗
	Gas diffusion coefficient in water	D_{water}	cm^2/s	✓	✗	✗
Biochemical	Apparent permeability (epithelium)	P_{epi}	cm/s	✓	✓	✓
	Apparent permeability (endothelium)	$P_{\text{endo,lung}}$	cm/s	✓	✓	✓
	Permeability-area product (endothelium)[c]	$PA_{\text{endo},t}$	mL/s	✓	✓	✓
	Fraction unbound in plasma	f_{up}	—	✓	✓	✓
	Tissue to plasma (unbound) partition coefficients[c]	$K_{\text{T2pu},t}$	—	✓	✓	✓
	Red blood cell to plasma (unbound) partition coefficient	K_{RBC2pu}	—	✓	✓	✓
	Dissolution rate constant in lining fluid	k_{dis}	μm/h	✗	✗	✓
	Dissolution rate constant in macrophages	$k_{\text{dis,MP}}$	μm/h	✗	✗	✓
	Intrinsic hepatic clearance	Cl_{int}	mL/h	✓	✓	✓
	Biliary clearance rate constant	k_{bile}	h^{-1}	✓	✓	✓
	Fraction of peritubular reabsorption	$f_{\text{reabsorption}}$	—	✓	✓	✓
	Fraction of peritubular secretion	$f_{\text{secretion}}$	—	✓	✓	✓

Note: Required input parameters depend on the type of the inhaled compounds, being either a gas/vapor, droplet or particle aerosol.
[a]For all model compartments j.
[b]For all 25 lung generations.
[c]For all modeled tissues t (e.g., lung, liver, spleen, and so forth).

All remaining model inputs listed in Table S1 have negligible impact on uptake. Arbitrary values were picked for them or set to zero to deactivate their respective processes.

3 | Results

The inhalation of gases and aerosolized particles was evaluated separately in two studies. Droplets were not explicitly explored, as they behave kinetically similar to nearly instantaneously dissolving particles or gases, once deposited onto the lining fluid. Particles were applied as a bolus while vapor uptake was modeled for continuous exposure.

The two studies assess the impact of substance-specific input parameters, as well as typical model assumptions; these are:

- Parameter study on gas/vapor absorption (continuous exposure)—investigates the impact of Henry's law constant and the diffusion coefficient in air on different absorption mechanisms to predict lung and blood concentrations.
- Parameter study on particle retention (bolus application)—demonstrates how alveolar macrophages influence particle retention in the deep lung due to long-term clearance or phagolysosome-aided dissolution.

3.1 | Parameter Study on Gas/Vapor Absorption

Figure 2 shows the predicted lung lumen concentration of the trachea (G1) and alveoli (G25) for a 30 min exposure duration to 100 mg/m^3 of a hypothetical gaseous substance. Median values for Henry's law constant and diffusion coefficient exemplify the

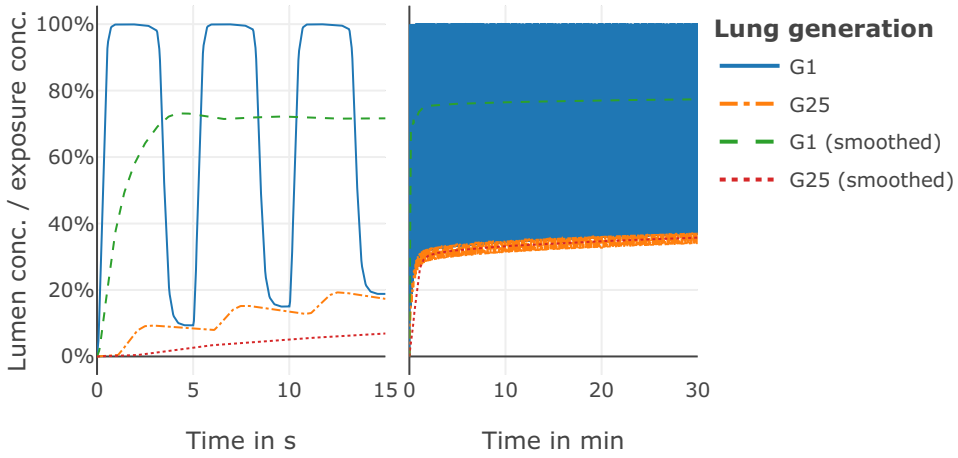

FIGURE 2 | Predicted ratio of lumen to external air concentration during inhalation of a hypothetical gas (100 mg/m^3) in generation 1 (trachea) and 25 (alveoli) for median values of Henry's law constant, air diffusion coefficient and fast lung permeation. Left: Initial filling of airways during the first three breaths. Right: Quasi-steady state and transitional phase.

most common case study. Due to cycling breathing, concentrations fluctuate breath-by-breath but eventually equilibrate into a quasi-steady state. The passage of the inhaled gas from the trachea to the alveoli is evident by a 1–2 s time delay of breath-by-breath peak concentrations.

Gas concentrations peak during inhalation and are lowest during exhalation. Note that in the following results, smoothed values are plotted instead of the actual, fluctuating values.

Plausible values of Henry's law constant and air diffusion coefficient were used to simulate gas absorption of a hypothetical gas during a 30-min exposure to 100 mg/m^3. Figure 3 shows predicted lung lumen and ELF concentrations and the transfer rate from lumen to fluid across time and all lung generations. Comparing low ($7.30 \cdot 10^{-7}$ mol/Pa/m^3), median ($1.60 \cdot 10^{-2}$ mol/Pa/m^3), and high ($5.92 \cdot 10^{2}$ mol/Pa/m^3) Henry's law constant with a constant median diffusion coefficient indicates its major impact on the resulting model outputs. Substances with a low Henry's law constant equilibrate rapidly in the lung lumen and ELF, with minimal uptake in the ELF, primarily occurring in G25.

Median values yield higher ELF concentrations and increased absorption in pulmonary generations. Gas concentrations in the lumen are below the ambient exposure concentration and lowest where absorption is highest.

High Henry's law constants result in lower lumen gas concentrations, with no gas reaching the pulmonary region. ELF concentrations peak in bronchiolar regions (G9–G16) and drop sharply due to high absorption in richly perfused pulmonary tissues (G17–G18), which result in fast drainage from lining fluid over tissue into blood.

Total absorption at quasi-steady-state is approximately $2.7 \cdot 10^{-3}$, 22, and 45 mg/h for low, median, and high Henry's law constants, respectively. Radial diffusion leads to both absorption and desorption, with desorption reducing uptake by up to 15% initially and settling to 10% or none during quasi-steady-state, depending on the Henry's law constant (Figure 4A).

The Henry's law constant strongly affects ELF and blood concentrations, while the diffusion coefficient has minimal effect on blood concentrations due to the rate-limiting transport across the tissue barrier (Figure 4B). The diffusion coefficient shows a strong effect on ELF concentrations in conjunction with a high Henry's law constant.

3.2 | Parameter Study on Particle Retention

To assess clearance processes' impact on lung burden, that is the total amount of deposited particles over time, a bolus inhalation of 10 mg of monodisperse, bioinert particles (MMAD: 2 μm) was modeled. Of the 10 mg, 88% was predicted by the MPPD model to deposit in the lung.

Figure 5 (bottom) depicts predicted total lung burden as a fraction of initially deposited particles during the fast clearance phase. Lung retention per generation is shown in Figure S5. Approximately 22% of the initial dose is cleared within 48 h via mucociliary mechanisms. In the deep lung, nearly all particles are captured by alveolar macrophages within the same period. Afterward, dynamic equilibrium between phagocytosis and apoptosis is reached, leaving ~2.7% of free particles on the lung's surface.

Figure 5 (top) illustrates the slow clearance phase, with a typical half-life of 250 days for different particle sizes. After rapid clearance in the first 2 days (inset), particles are slowly removed via macrophages exiting the trachea. The transition between fast and slow clearance depends on particle deposition ratios between tracheobronchial and pulmonary regions, influenced by particle size. Larger particles (e.g., 10 μm) represent the upper limit for alveolar deposition [29].

To evaluate dissolution impacts, model predictions spanned dissolution rates from $1 \cdot 10^{-8}$ to $1 \cdot 10^{2}$ μg/h/cm^2. Figure 6 shows lung retention for particles dissolving in epithelial lining or phagolysosomal fluid. After the first day, dissolution rates spanning roughly two orders of magnitude (0.1–10 μg/h/cm^2) significantly impact retention. Below or above this range, any dissolution rate will either

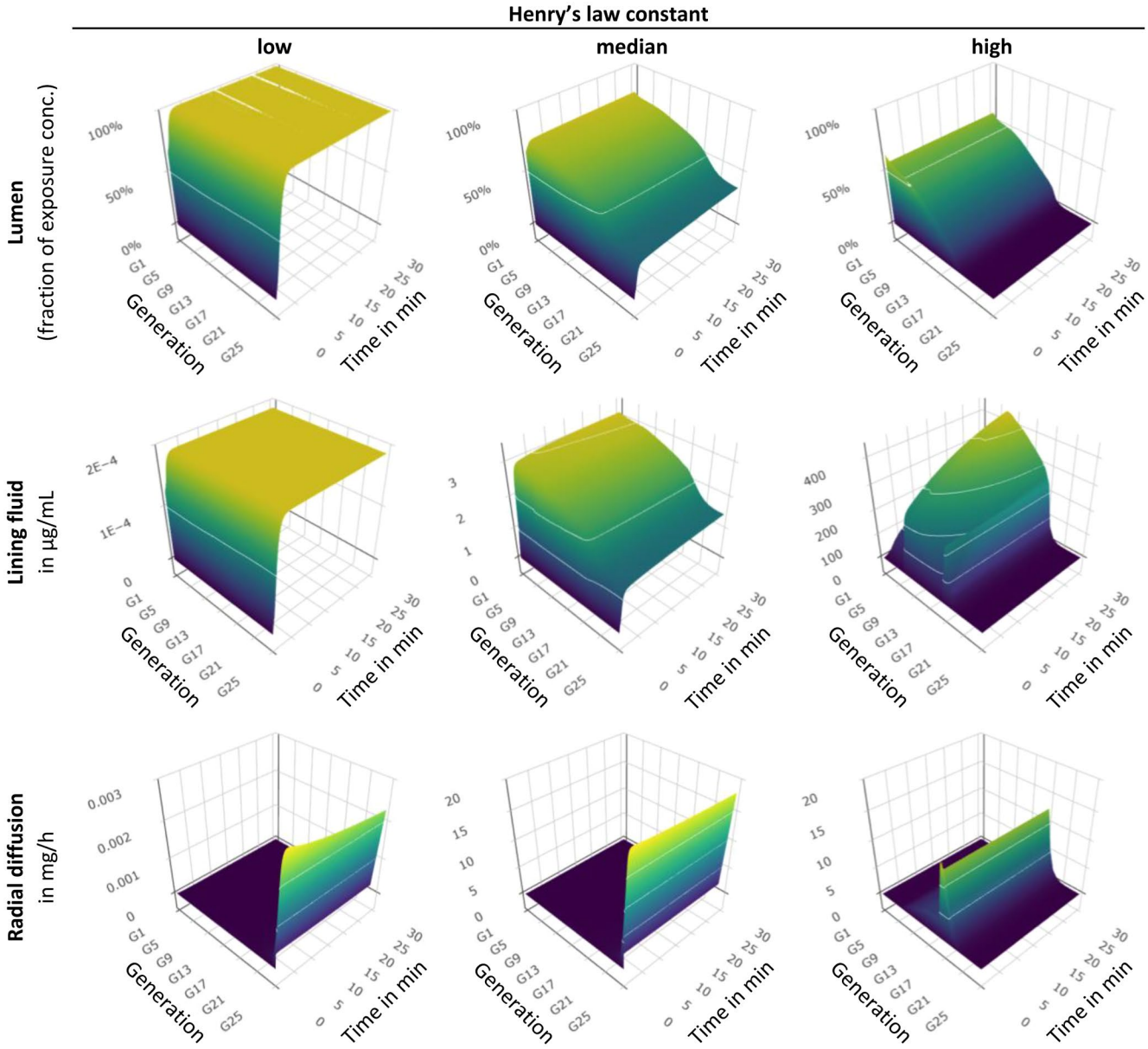

FIGURE 3 | Concentration and radial mass transfer rates in each lung generation during constant exposure compared for different Henry's law constant and continuous exposure to 100 mg/m^3 of a hypothetical gas.

have negligible influence on lung retention or completely dissolve all particles. Outside this range, dissolution rates either have negligible effects or completely dissolve particles. For macrophage-mediated dissolution, the critical range shifts to lower rates over a year. Predictions for lining fluid dissolution beyond 24 h were not made, as particles are nearly completely phagocytized at this point and are no longer exposed to lining fluid.

4 | Discussion

4.1 | Model Structure

The presented PBK model offers a detailed framework to predict local concentrations within the lung, enabling evaluation of concentration–time profiles for individual airway generations.

4.1.1 | Key Mechanisms

Unlike earlier models, which relied on plug flow assumptions and overlooked diffusion effects [8], this model incorporates longitudinal diffusion between air compartments. This inclusion allows substances to mix between tidal air and residual air, ensuring deeper lung penetration even under shallow breathing or breath-holding scenarios.

The transition from convective to diffusional flow, a phenomenon captured by the Peclet number, occurs around generation 18 in this model (Figure S3), aligning with literature for resting individuals [30]. The gradual dominance of diffusion over convection in distal airways minimizes fluctuations in lumen concentrations compared to proximal airways, influenced by both absorption into lining fluid and mixing between airway generations (Figure 2).

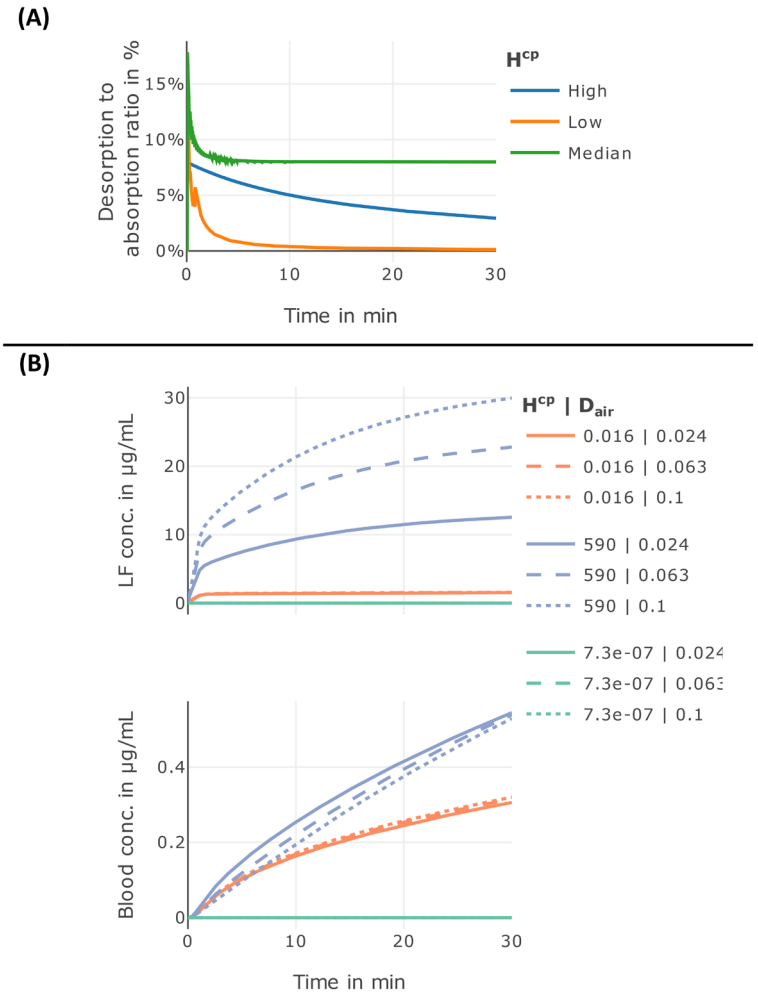

FIGURE 4 | (A) Wash-in/wash-out effect for different Henry's law constant (Hcp) shown as the ratio of cumulative desorption and absorption from/to the lining fluid and the gas phase over time during inhalation of a hypothetical gas (100 mg/m^3). (B) Volume-weighted mean concentration in lining fluid across all airway generations (left) and blood concentrations (right) for different Henry's law constants (mol/Pa/m^3) and diffusion coefficients (cm^2/s) during constant exposure of 100 mg/m^3 of a hypothetical gas.

For aerosols, the model extends beyond the typical focus on either insoluble particles [31] or rapidly dissolving particles [16, 17]. It incorporates macrophage-assisted dissolution, an often-overlooked process in risk assessments [32]. While in vitro dissolution tests commonly use artificial lining fluids, they fail to replicate the acidic environment of phagolysosomes, which can significantly alter dissolution kinetics [18]. This capability is particularly relevant for understanding long-term particle retention and bioaccumulation in the deep lung or for evaluating pharmaceutical delivery systems targeting macrophages [33].

The model tracks multiple particle metrics, that is, size, mass, number, and surface area, providing insights into toxicological and pharmacological mechanisms [34, 35]. These metrics can be calculated for each airway generation and expressed relative to local surface areas. However, the current implementation tracks only single-sized particles, limiting its applicability to scenarios involving bolus injections or uniform dissolution rates. Integrating algorithms to handle particle size distributions would expand the model's scope to continuous inhalation of variable-sized particles or different dissolution rates across compartments [16, 17, 36].

4.1.2 | Model Assumptions and Limitations

Several assumptions and limitations in the current model implementation should be noted:

- The presented PBK model only includes the lower respiratory tract (i.e., the lung). The upper respiratory tract and therefore mucosal absorption via the larynx, pharynx, nasal airways, or the mouth cavity are not considered.
- Whole lung models cannot be validated on the level of airway generations. Experimental in vivo data on lung uptake or retention is currently only available for the lung in its entirety.
- Morphometric data are based on a single lung cast [20, 37], limiting its representativeness for diverse populations.
- Only passive diffusion across the epithelial barrier is modeled, excluding membrane transporters and active transport.
- Clearance in ELF or lung tissue due to chemical reactions or metabolic degradation is not included, though these can be integrated in future iterations [10, 38].

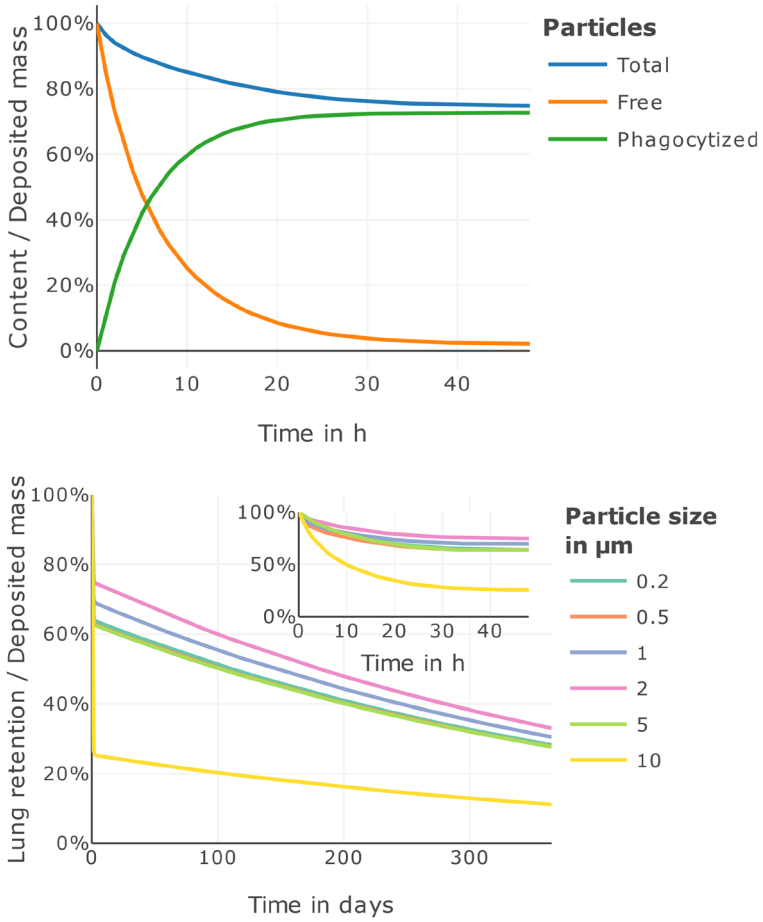

FIGURE 5 | Particle retention in the lung after bolus application of bioinert particles. Top: Short-term clearance of inhaled particles (2 µm). Within 24 h, particles deposited in the upper lung (G1–G16) are cleared via the mucociliary escalator while particles in the deep lung are phagocytized. At equilibrium, a small quantity of particles remains always uncaptured. Bottom: Slow clearance particles with different particle sizes. Inset: The corresponding lung retention during the short-term clearance phase (within 48 h).

- The diffusional exchange area between capillary blood and lung tissue assumes complete capillary recruitment. Complete recruitment occurs due to increased lung perfusion and blood pressure and may not reflect resting conditions.
- The Henry's law constant is per definition only valid for low molar fractions in a fluid.
- Dissolution assumes single-species solubility, excluding cases involving multiple dissolution products. In these cases, only lung burden (under sink conditions for the dissolved species) can be computed.
- Stained pulmonary lymph nodes indicate particles can cross the epithelial barrier into interstitial spaces, potentially moving to the lymph system or blood [39]. However, the mechanisms and rates remain unclear, and translocation has minimal impact on overall particle fate [40]. For these reasons, translocation is not modeled.

4.2 | Parameter Studies

The model was applied to hypothetical vapor and aerosol scenarios to investigate key mechanisms influencing inhalational uptake and lung retention.

4.2.1 | Vapor Uptake

Vapor concentration-time curves follow three characteristic phases: quasi-steady-state absorption, transitional equilibrium, and steady-state clearance [41]. The first two phases were observed in the study (Figure 2), with Henry's law constant identified as a critical determinant of lung concentrations (Figure 3):

- Low Henry's law constant: Limited absorption occurs due to low lining fluid concentrations, with most uptake confined to the alveolar region. This behavior is in line with the well-known properties of oxygen, a typical gas with a low Henry's law constant of $1.3 \cdot 10^{-5}$ mol/m^3/Pa [25] which is also mainly absorbed in the alveolar region.
- Median Henry's law constant: Higher lining fluid concentrations enable faster diffusion across the cell barrier, shifting uptake to be limited by tidal volume and breathing frequency. This shift becomes more apparent using very high Henry's law constants.
- High Henry's law constant: Rapid absorption in transitional airways prevents substantial penetration into the pulmonary region, emphasizing the role of radial diffusion. This is also

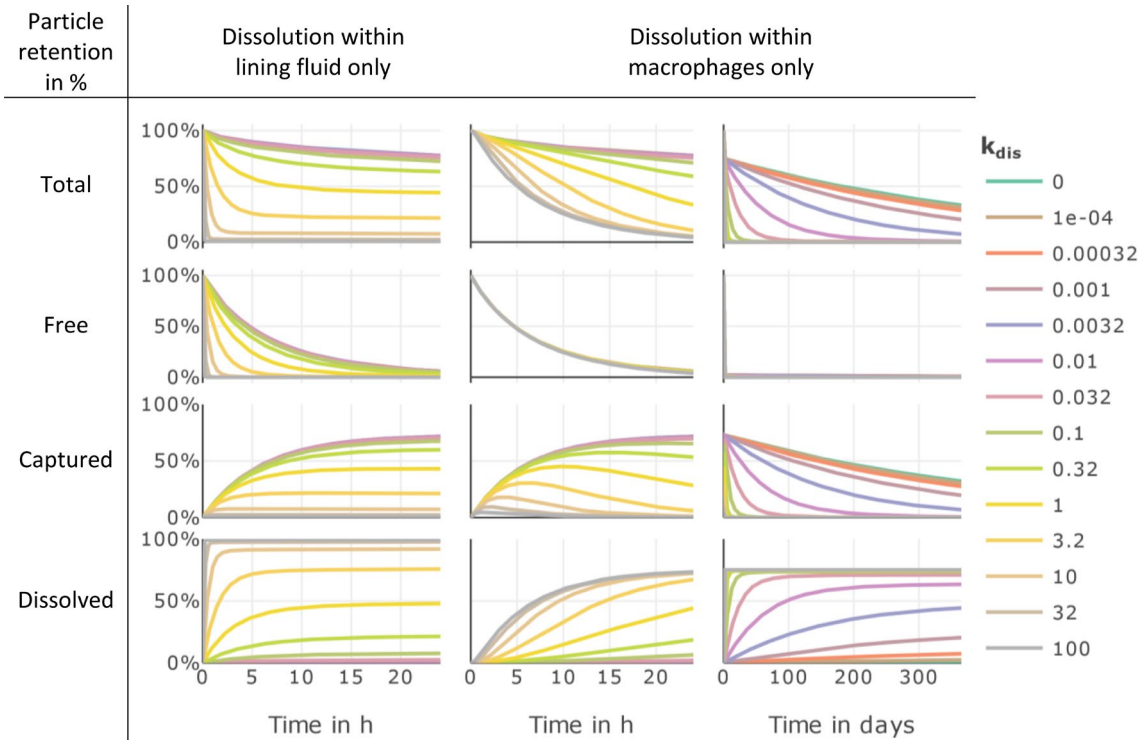

FIGURE 6 | Influence of particle dissolution rates (μg/h/cm^2) within lining fluid or alveolar macrophages on lung retention. Shown is the retention of particles (MMAD = 2 μm) deposited in the alveolar region for 24 h and 360 days. Particles are either free on the alveolar surface, captured within macrophages, or dissolved (total = free + captured + dissolved).

apparent in the increasing mean concentration in lining fluid, although blood concentrations are unaffected (Figure 4B).

The wash-in/wash-out effect [9, 42], that is, initial absorption followed by partial desorption, is evident for substances with median and high Henry's law constants (Figure 4A). Simpler models that assume instant equilibrium between gas and tissue are unsuitable for such substances, as they fail to account for desorption dynamics in upper airways.

4.2.2 | Particle Retention and Clearance

Predicted particle retention after 48 h (~2.7%) (Figure 5) aligns with clinical observations (~3.5%) [43] but underestimates total retention, possibly due to the omission of exocytosis as a release mechanism [44, 45].

Predicted clearance by mucociliary and macrophage-mediated removal (Figure 5) was consistent with empirical data, though particle properties such as size and surface charge may influence these rates. Nano-sized particles, for example, are captured randomly via pinocytosis rather than chemotactic attraction, which affects their clearance efficiency [46]. Depending on their size and surface charge, particles might avoid mucociliary clearance by penetrating the mobile gel layer into the stationary sol layer beneath [47].

Model results indicate that lung burden predictions after 24 h are most sensitive to dissolution rates between 0.01 and 70 μg/h/cm^2 (Figure 6). These findings require further validation. Low solubility or slow drainage of dissolved material from ELF may abruptly halt dissolution. Additionally, this model assumes spherical particles, excluding effects from agglomeration or non-spherical shapes, that is, phagocytosis impairing fibrous asbestos [48, 49]. Additionally, the limits found here vary with different endpoints; for example, after 24 h, slow macrophage clearance has minimal impact. Over a year, particles with dissolution rates above 0.01 μg/h/cm^2 are largely cleared, with three-quarters dissolved and the remainder removed by macrophages (Figure 6).

4.3 | Limitations of Parameter Studies

A full sensitivity analysis, as recommended by OECD guidance [6], was not conducted due to substance-specific variability. Analyzing a hypothetical substance can misrepresent the importance of individual parameters due to the complexity of inhalational uptake, influenced by numerous factors. Covering all variations is beyond this publication's scope. The presented results are generalizable only to a certain extent and are intended as rough guidance for predicting outcomes based on specific substance properties. Factors like solubility and diffusion can become limiting under specific conditions. Changing tidal volume or breathing patterns may also significantly affect outcomes.

5 | Conclusion

The presented physiologically based kinetic (PBK) model offers a unified framework to predict inhalational uptake of gases, vapors, and aerosols. By dividing the lung into multiple compartments representing the 25 airway generations of the respiratory tree, the model accounts for mechanisms relevant to a broad

range of physicochemical properties of inhaled substances. In total, the model comprises 81 compartments, including 25 each for the airway lumen, particles, and epithelial lining fluid, along with compartments for tissues, blood, and alveolar macrophages.

Despite its detailed structure, the model requires relatively few additional parameters, especially when focused on a single substance class (e.g., gases/vapors or particles). Input requirements are designed to align with data obtainable from NAMs, enabling full QIVIVE or bottom-up applications.

Parameter studies have demonstrated the model's utility. For gases and vapors, variations in Henry's law constant and air diffusion coefficients elucidate their effects on absorption mechanisms, predicting both local lung and systemic concentrations. For particles, the role of alveolar macrophages in long-term retention and phagolysosome-aided dissolution underscores their importance in deep-lung particle clearance. These studies highlight the necessity of a compartmentalized lung structure, as concentrations vary significantly across airway generations. The model provides detailed predictions, including gas uptake, particle retention, and epithelial lining fluid concentrations for each airway generation, as well as systemic concentrations and extrapulmonary tissue distribution.

The model spans a wide application domain, covering insoluble and soluble gases as well as bioinert and fast-dissolving particles, making it a valuable tool for toxicologists and pharmacologists. It supports forward dosimetry for assessing local lung effects such as those from chemicals or targeted drug delivery. Further use cases include guiding animal study designs, evaluating aggregate exposures, performing reverse dosimetry to estimate airborne concentrations, analyzing bioaccumulation during repeated exposures, modeling single-breath uptake, and estimating exhaled breath concentrations.

This PBK model represents an advancement toward a standardized framework for inhalational uptake. Designed to be both generalizable and extensible, it provides a foundation for further refinement and broader applications in toxicological and pharmacological research.

Author Contributions

N.N. wrote the manuscript; N.N., S.E.E., and K.S. designed the research; N.N. performed the research; N.N., S.E.E., and K.S. analyzed the data, and N.N. contributed new analytical tools.

Acknowledgments

Special thanks to Prof. Dr. Wolfgang Koch for his support and invaluable insights in aerosol physics. Open Access funding enabled and organized by Projekt DEAL.

Conflicts of Interest

The authors declare no conflicts of interest.

References

1. A. R. Kolli, A. K. Kuczaj, F. Martin, A. W. Hayes, M. C. Peitsch, and J. Hoeng, "Bridging Inhaled Aerosol Dosimetry to Physiologically Based Pharmacokinetic Modeling for Toxicological Assessment: Nicotine Delivery Systems and Beyond," *Critical Reviews in Toxicology* 49, no. 9 (2019): 725–741, https://doi.org/10.1080/10408444.2019.1692780.

2. A. Punt, H. Bouwmeester, B. J. Blaauboer, et al., "New Approach Methodologies (NAMs) for Human-Relevant Biokinetics Predictions. Meeting the Paradigm Shift in Toxicology Towards an Animal-Free Chemical Risk Assessment," *ALTEX* 37, no. 4 (2020): 607–622, https://doi.org/10.14573/altex.2003242.

3. S. E. Escher, F. Partosch, S. Konzok, et al., "Development of a Roadmap for Action on New Approach Methodologies in Risk Assessment," *EFS3* 19, no. 6 (2022): 26–45, https://doi.org/10.2903/sp.efsa.2022.EN-7341.

4. J. G. Bessems, G. Loizou, K. Krishnan, et al., "PBTK Modelling Platforms and Parameter Estimation Tools to Enable Animal-Free Risk Assessment: Recommendations From a Joint EPAA–EURL ECVAM ADME Workshop," *Regulatory Toxicology and Pharmacology* 68, no. 1 (2014): 119–139, https://doi.org/10.1016/j.yrtph.2013.11.008.

5. J. L. Campbell, R. A. Clewell, P. R. Gentry, M. E. Andersen, and H. J. Clewell, "Physiologically Based Pharmacokinetic/Toxicokinetic Modeling," *Methods in Molecular Biology* 929 (2012): 439–499, https://doi.org/10.1007/978-1-62703-050-2_18.

6. OECD, *Guidance Document on the Characterisation, Validation and Reporting of Physiologically Based Kinetic (PBK) Models for Regulatory Purposes*, 331st ed. (Environment, Health and Safety, Environment Directorate, OECD, 2021). OECD Series on Testing and Assessment.

7. Y. Henderson and H. W. Haggard, *Noxious Gases and the Principles of Respiration Influencing Their Action*, 2nd ed. (Reinhold Publishing Corporation, 1943).

8. A. Vinegar, G. W. Jepson, and J. H. Overton, "PBPK Modeling of Short-Term (0–5 Min) Human Inhalation Exposures to Halogenated Hydrocarbons," *Inhalation Toxicology* 10, no. 5 (1998): 411–429, https://doi.org/10.1080/089583798197600.

9. G. Johanson, "Modelling of Respiratory Exchange of Polar Solvents," *Annals of Occupational Hygiene* 35, no. 3 (1991): 323–339, https://doi.org/10.1093/annhyg/35.3.323.

10. R. Sarangapani, J. G. Teeguarden, G. Cruzan, H. J. Clewell, and M. E. Andersen, "Physiologically Based Pharmacokinetic Modeling of Styrene and Styrene Oxide Respiratory-Tract Dosimetry in Rodents and Humans," *Inhalation Toxicology* 14, no. 8 (2002): 789–834, https://doi.org/10.1080/08958370290084647.

11. R. Z. Boerleider, J. D. N. Olie, J. C. H. van Eijkeren, et al., "Evaluation of Three Physiologically Based Pharmacokinetic (PBPK) Modeling Tools for Emergency Risk Assessment After Acute Dichloromethane Exposure," *Toxicology Letters* 232, no. 1 (2015): 21–27, https://doi.org/10.1016/j.toxlet.2014.10.010.

12. M. W. Linakis, R. R. Sayre, R. G. Pearce, et al., "Development and Evaluation of a High Throughput Inhalation Model for Organic Chemicals," *Journal of Exposure Science & Environmental Epidemiology* 30, no. 5 (2020): 866–877, https://doi.org/10.1038/s41370-020-0238-y.

13. ICRP, "Human Respiratory Tract Model for Radiological Protection. A Report of a Task Group of the International Commission on Radiological Protection," *Annals of the ICRP* 24, no. 1–3 (1994): 1–482.

14. F. Paquet, G. Etherington, M. R. Bailey, et al., "ICRP Publication 130: Occupational Intakes of Radionuclides: Part 1," *Annals of the ICRP* 44, no. 2 (2015): 5–188, https://doi.org/10.1177/0146645315577539.

15. L. Gaohua, J. Wedagedera, B. G. Small, et al., "Development of a Multicompartment Permeability-Limited Lung PBPK Model and Its Application in Predicting Pulmonary Pharmacokinetics of Antituberculosis Drugs," *CPT: Pharmacometrics & Systems Pharmacology* 4, no. 10 (2015): 605–613, https://doi.org/10.1002/psp4.12034.

16. E. Boger and O. Wigström, "A Partial Differential Equation Approach to Inhalation Physiologically Based Pharmacokinetic Modeling," *CPT:*

Pharmacometrics & Systems Pharmacology 7, no. 10 (2018): 638–646, https://doi.org/10.1002/psp4.12344.

17. N. Hartung and J. M. Borghardt, "A Mechanistic Framework for a Priori Pharmacokinetic Predictions of Orally Inhaled Drugs," *PLoS Computational Biology* 16, no. 12 (2020): e1008466, https://doi.org/10.1371/journal.pcbi.1008466.

18. E. Innes, H. H. P. Yiu, P. McLean, W. Brown, and M. Boyles, "Simulated Biological Fluids—A Systematic Review of Their Biological Relevance and Use in Relation to Inhalation Toxicology of Particles and Fibres," *Critical Reviews in Toxicology* 51, no. 3 (2021): 217–248, https://doi.org/10.1080/10408444.2021.1903386.

19. M. Gorguner and M. Akgun, "Acute Inhalation Injury," *Eurasian Journal of Medicine* 42, no. 1 (2010): 28–35, https://doi.org/10.5152/eajm.2010.09.

20. H. C. Yeh and G. M. Schum, "Models of Human Lung Airways and Their Application to Inhaled Particle Deposition," *Bulletin of Mathematical Biology* 42, no. 3 (1980): 461–480.

21. E. M. Wagner, "Bronchial Circulation," in *Reference Module in Biomedical Sciences* (Elsevier, 2020).

22. B. Corrin and A. G. Nicholson, "The Structure of the Normal Lungs," in *Pathology of the Lungs* (Elsevier, 2011), 1–37.

23. K. Soetaert, T. Petzoldt, and R. W. Setzer, "Solving Differential Equations in R: Package deSolve," *Journal of Statistical Software* 33, no. 9 (2010): 1–25, https://doi.org/10.18637/jss.v033.i09.

24. ICRP, "Basic Anatomical and Physiological Data for Use in Radiological Protection: Reference Values," A Report of Age- and Gender-Related Differences in the Anatomical and Physiological Characteristics of Reference Individuals, ICRP Publication 89, *Annals of the ICRP* 32, no. 3–4 (2002): 5–265.

25. R. Sander, "Compilation of Henry's Law Constants (Version 4.0) for Water as Solvent," *Atmospheric Chemistry and Physics* 15, no. 8 (2015): 4399–4981, https://doi.org/10.5194/acp-15-4399-2015.

26. C. L. Yaws, *Transport Properties of Chemicals and Hydrocarbons: Viscosity, Thermal Conductivity, and Diffusivity of C1 to C100 Organics and ac to Zr Inorganics* (William Andrew, 2009).

27. S. Anjilvel and B. Asgharian, "A Multiple-Path Model of Particle Deposition in the Rat Lung," *Fundamental and Applied Toxicology* 28, no. 1 (1995): 41–50, https://doi.org/10.1006/faat.1995.1144.

28. T. Pasman, D. Baptista, S. van Riet, et al., "Development of an In Vitro Airway Epithelial–Endothelial Cell Culture Model on a Flexible Porous Poly(Trimethylene Carbonate) Membrane Based on Calu-3 Airway Epithelial Cells and Lung Microvascular Endothelial Cells," *Membranes* 11, no. 3 (2021): 197, https://doi.org/10.3390/membranes11030197.

29. G. Oberdörster, E. Oberdörster, and J. Oberdörster, "Nanotoxicology: An Emerging Discipline Evolving From Studies of Ultrafine Particles," *Environmental Health Perspectives* 113, no. 7 (2005): 823–839, https://doi.org/10.1289/ehp.7339.

30. F. Noël and B. Mauroy, "Interplay Between Optimal Ventilation and Gas Transport in a Model of the Human Lung," *Frontiers in Physiology* 10 (2019): 488, https://doi.org/10.3389/fphys.2019.00488.

31. G. P. Gakis, A. Krikas, P. Neofytou, L. Tran, and C. Charitidis, "Modelling the Biodistribution of Inhaled Gold Nanoparticles in Rats With Interspecies Extrapolation to Humans," *Toxicology and Applied Pharmacology* 457 (2022): 116322, https://doi.org/10.1016/j.taap.2022.116322.

32. J. G. Keller, U. M. Graham, J. Koltermann-Jülly, et al., "Predicting Dissolution and Transformation of Inhaled Nanoparticles in the Lung Using Abiotic Flow Cells: The Case of Barium Sulfate," *Scientific Reports* 10, no. 1 (2020): 458, https://doi.org/10.1038/s41598-019-56872-3.

33. B. Patel, N. Gupta, and F. Ahsan, "Particle Engineering to Enhance or Lessen Particle Uptake by Alveolar Macrophages and to Influence the Therapeutic Outcome," *European Journal of Pharmaceutics and Biopharmaceutics* 89 (2015): 163–174, https://doi.org/10.1016/j.ejpb.2014.12.001.

34. O. Schmid and T. Stoeger, "Surface Area Is the Biologically Most Effective Dose Metric for Acute Nanoparticle Toxicity in the Lung," *Journal of Aerosol Science* 99 (2016): 133–143, https://doi.org/10.1016/j.jaerosci.2015.12.006.

35. J. Pauluhn, "Poorly Soluble Particulates: Searching for a Unifying Denominator of Nanoparticles and Fine Particles for DNEL Estimation," *Toxicology* 279, no. 1–3 (2011): 176–188, https://doi.org/10.1016/j.tox.2010.10.009.

36. A. L. Dale, G. V. Lowry, and E. A. Casman, "Accurate and Fast Numerical Algorithms for Tracking Particle Size Distributions During Nanoparticle Aggregation and Dissolution," *Environmental Science: Nano* 4, no. 1 (2017): 89–104, https://doi.org/10.1039/C6EN00330C.

37. O. G. Raabe, H.-C. Yeah, M. G. Schum, and R. F. Phalen, "Tracheobronchial Geometry: Human, Dog, Rat, Hamster: A Compilation of Selected Data From the Project Respiratory Tract Deposition Models," (1976).

38. M. K. Ladumor and J. D. Unadkat, "Predicting Regional Respiratory Tissue and Systemic Concentrations of Orally Inhaled Drugs Through a Novel PBPK Model," *Drug Metabolism and Disposition* 50, no. 5 (2022): 519–528, https://doi.org/10.1124/dmd.121.000789.

39. B. B. Ural, D. P. Caron, P. Dogra, et al., "Inhaled Particulate Accumulation With Age Impairs Immune Function and Architecture in Human Lung Lymph Nodes," *Nature Medicine* 28, no. 12 (2022): 2622–2632, https://doi.org/10.1038/s41591-022-02073-x.

40. A. Kermanizadeh, D. Balharry, H. Wallin, S. Loft, and P. Møller, "Nanomaterial Translocation—The Biokinetics, Tissue Accumulation, Toxicity and Fate of Materials in Secondary Organs—A Review," *Critical Reviews in Toxicology* 45, no. 10 (2015): 837–872, https://doi.org/10.3109/10408444.2015.1058747.

41. J. B. Morris, "Biologically-Based Modeling Insights in Inhaled Vapor Absorption and Dosimetry," *Pharmacology & Therapeutics* 136, no. 3 (2012): 401–413, https://doi.org/10.1016/j.pharmthera.2012.08.017.

42. S. Kumagai and I. Matsunaga, "A Lung Model Describing Uptake of Organic Solvents and Roles of Mucosal Blood Flow and Metabolism in the Bronchioles," *Inhalation Toxicology* 12, no. 6 (2000): 491–510, https://doi.org/10.1080/089583700402888.

43. J. C. Lay, W. D. Bennett, C. S. Kim, R. B. Devlin, and P. A. Bromberg, "Retention and Intracellular Distribution of Instilled Iron Oxide Particles in Human Alveolar Macrophages," *American Journal of Respiratory Cell and Molecular Biology* 18, no. 5 (1998): 687–695, https://doi.org/10.1165/ajrcmb.18.5.2948.

44. B. D. Chithrani and W. C. W. Chan, "Elucidating the Mechanism of Cellular Uptake and Removal of Protein-Coated Gold Nanoparticles of Different Sizes and Shapes," *Nano Letters* 7, no. 6 (2007): 1542–1550, https://doi.org/10.1021/nl070363y.

45. H. C. Fischer, T. S. Hauck, A. Gómez-Aristizábal, and W. C. W. Chan, "Exploring Primary Liver Macrophages for Studying Quantum Dot Interactions With Biological Systems," *Advanced Materials* 22, no. 23 (2010): 2520–2524, https://doi.org/10.1002/adma.200904231.

46. S. Moreno-Mendieta, D. Guillén, N. Vasquez-Martínez, R. Hernández-Pando, S. Sánchez, and R. Rodríguez-Sanoja, "Understanding the Phagocytosis of Particles: The Key for Rational Design of Vaccines and Therapeutics," *Pharmaceutical Research* 39, no. 8 (2022): 1823–1849, https://doi.org/10.1007/s11095-022-03301-2.

47. Q. Liu, J. Guan, L. Qin, X. Zhang, and S. Mao, "Physicochemical Properties Affecting the Fate of Nanoparticles in Pulmonary Drug Delivery," *Drug Discovery Today* 25, no. 1 (2020): 150–159, https://doi.org/10.1016/j.drudis.2019.09.023.

48. T. Ishida, N. Fujihara, T. Nishimura, et al., "Live-Cell Imaging of Macrophage Phagocytosis of Asbestos Fibers Under Fluorescence Microscopy," *Genes and Environment* 41 (2019): 14, https://doi.org/10.1186/s41021-019-0129-4.

49. D. Paul, S. Achouri, Y.-Z. Yoon, J. Herre, C. E. Bryant, and P. Cicuta, "Phagocytosis Dynamics Depends on Target Shape," *Biophysical Journal* 105, no. 5 (2013): 1143–1150, https://doi.org/10.1016/j.bpj.2013.07.036.

Supporting Information

Additional supporting information can be found online in the Supporting Information section. **Appendix S1:** psp470117-sup-0001-AppendixS1.xlsx. **Appendix S2:** psp470117-sup-0002-AppendixS2.docx.